An Epigenetic Signature for Monoallelic Olfactory Receptor Expression

Angeliki Magklara,[1] Angela Yen,[4,5,7] Bradley M. Colquitt,[2,7] E. Josephine Clowney,[3,7] William Allen,[6] Eirene Markenscoff-Papadimitriou,[2] Zoe A. Evans,[1] Pouya Kheradpour,[4,5] George Mountoufaris,[1] Catriona Carey,[1] Gilad Barnea,[6] Manolis Kellis,[4,5] and Stavros Lomvardas[1,2,3,*]

[1]Department of Anatomy
[2]Program in Neurosciences
[3]Program in Biomedical Sciences
University of California, San Francisco, San Francisco, CA 94158, USA
[4]Broad Institute of MIT and Harvard, Cambridge, MA 02142, USA
[5]Computer Science and Artificial Intelligence Laboratory, MIT, Cambridge, MA 02139, USA
[6]Department of Neuroscience, Brown University, Providence, RI 02912, USA
[7]These authors contributed equally to this work
*Correspondence: stavros.lomvardas@ucsf.edu
DOI 10.1016/j.cell.2011.03.040

SUMMARY

Constitutive heterochromatin is traditionally viewed as the static form of heterochromatin that silences pericentromeric and telomeric repeats in a cell cycle- and differentiation-independent manner. Here, we show that, in the mouse olfactory epithelium, olfactory receptor (OR) genes are marked in a highly dynamic fashion with the molecular hallmarks of constitutive heterochromatin, H3K9me3 and H4K20me3. The cell type and developmentally dependent deposition of these marks along the OR clusters are, most likely, reversed during the process of OR choice to allow for monogenic and monoallelic OR expression. In contrast to the current view of OR choice, our data suggest that OR silencing takes place before OR expression, indicating that it is not the product of an OR-elicited feedback signal. Our findings suggest that chromatin-mediated silencing lays a molecular foundation upon which singular and stochastic selection for gene expression can be applied.

INTRODUCTION

In mammals, olfactory perception is accomplished by detection of volatile chemicals in the olfactory epithelium and transmission of the odorant information to the brain, where it is processed. Unlike other sensory systems, olfaction relies on a large family of OR genes that are expressed in a monogenic and monoallelic fashion in olfactory sensory neurons (OSNs) (Buck and Axel, 1991; Chess et al., 1994). OSNs that express the same OR converge to the same glomerulus in the olfactory bulb (Axel, 2005). ORs participate both in odor detection and in guiding the axons to the proper glomeruli, ascribing this way the func-

tional identity of each neuron (Imai et al., 2010). The dual role of ORs in the wiring and physiology of the olfactory system emphasizes the importance of their proper expression. Each neuron faces the challenging task of expressing one OR allele at high levels while keeping the rest of the repertoire completely silent. The effective repression of the nonchosen alleles is crucial for this system; due to the exceptionally high number of family members, basal transcription from the nonchosen ORs would result in thousands of inappropriately expressed OR molecules. Although each individual OR would have insignificant representation, all together they would generate OR activity comparable to the one from the chosen allele, likely resulting in wiring perturbations and subsequent sensory confusion.

In the mouse, ~1400 ORs are expressed in the main olfactory epithelium (MOE) in a spatial and temporal fashion that could be organized by positional cues. Within a zone of expression, however, each neuron expresses only one out of several hundred alleles that have the potential to be transcribed in that particular region in a seemingly stochastic fashion (Shykind, 2005). Genetic experiments suggest that the production of OR protein elicits a feedback signal that stabilizes the expression of the encoding allele and prevents the activation of additional OR genes (Lewcock and Reed, 2004; Serizawa et al., 2003; Shykind et al., 2004). Moreover, there is evidence that the OR coding sequence represses heterologous promoters, suggesting that it contains important information for the regulation of OR expression (Nguyen et al., 2007). Regulatory information is also included in proximal promoter sequences of OR genes, as well as in distant enhancer elements (Rothman et al., 2005; Serizawa et al., 2003). One of them, the H enhancer, interacts with active OR alleles in *cis* or *trans*, which led us to propose that this interaction might be instructive for OR expression (Lomvardas et al., 2006). However, genetic ablation of H disrupts the expression of only three proximal ORs, disputing a model in which H is a singular enhancer that orchestrates OR choice (Fuss et al., 2007; Nishizumi et al., 2007). Thus, despite immense
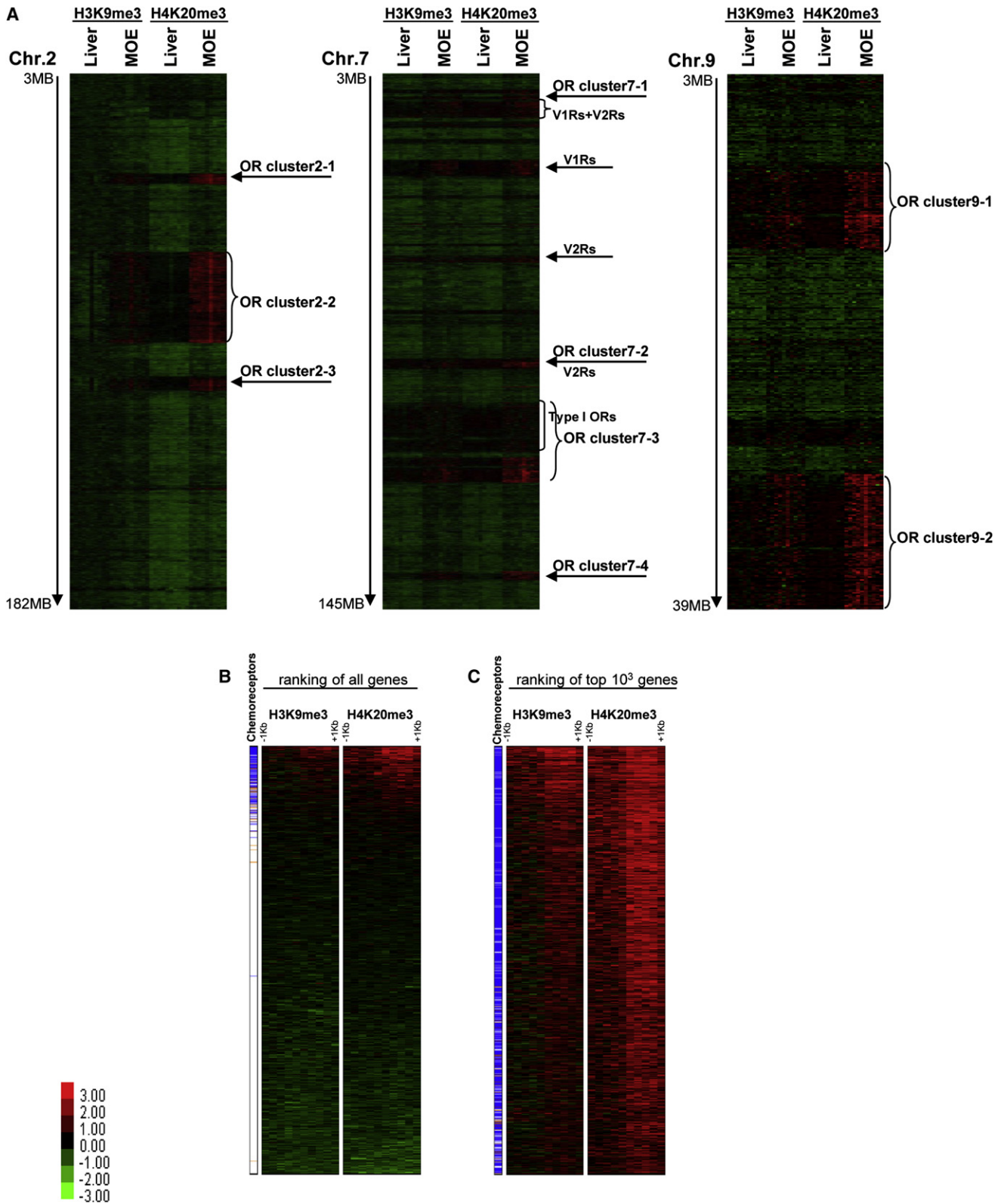
Figure 1. Genome-wide Mapping of H3K9me3 and H4K20me3 Reveals a Tissue-Dependent Heterochromatinization of the ORs in the MOE

ChIP-on-chip experiments with antibodies against H3K9me3 and H4K20me3 using native chromatin preparations from the MOE and liver. The log2 ratio of IP/input was calculated and used for the construction of the heatmaps presented here.

efforts, the molecular mechanisms regulating the activation of one OR allele and the stable transcriptional repression of the rest remain unknown.

Chromatin-mediated silencing constitutes an effective form of transcriptional repression. There are distinct forms of transcriptionally inactive chromatin known as heterochromatin. Facultative heterochromatin, a term assigned to the chromatin structure of silenced genes, is generally hypoacetylated and has di- and trimethyl groups on lysine 27 and/or dimethyl groups on lysine 9 of histone H3. This type of heterochromatin is dynamic and appears to be developmentally regulated (Trojer and Reinberg, 2007). In contrast, constitutive heterochromatin, characterized by the trimethylation of lysine 9 and lysine 20 of histones H3 and H4 (H3K9me3 and H4K20me3, respectively) is mostly found on pericentromeric and telomeric repeats and remains condensed during the cell cycle and stable during differentiation (Fodor et al., 2010).

Here, we test the hypothesis that chromatin-mediated silencing prevents the inappropriate expression of multiple OR genes in each sensory neuron. Our data show that, in the MOE, OR genes are subject to an unusual form of heterochromatic silencing that combines characteristics of both constitutive and facultative heterochromatin. Our ChIP-on-chip experiments reveal high levels of H3K9me3 and H4K20me3 on OR loci. The cell type and differentiation-dependent deposition of these trimethyl marks on OR clusters lead to the formation of compacted and inaccessible heterochromatic macrodomains. Surprisingly, heterochromatic compaction of OR clusters occurs before OR transcription and does not require OR expression, suggesting that it is not the product of an OR-elicited feedback signal. The enrichment for these silent marks is significantly reduced on an active OR allele, which is marked instead with trimethylated lysine 4 of histone H3 (H3K4me3). Insertion of a reporter transgene within such a heterochromatic macrodomain results in its effective chromatin-mediated silencing in the majority of the olfactory neurons and the subsequent OR-like expression of this transgene, indicating that stochastic escape from heterochromatic silencing could be the basis of monogenic and monoallelic gene expression.

RESULTS

Whole-Genome Analysis of H3K9me3 and H4K20me3 in the MOE

We performed chromatin immunoprecipitation (ChIP) experiments with antibodies against all methylated forms of H3K9, H3K27, and H4K20 using native chromatin preparations from MOE, hippocampus, liver, or mouse embryonic fibroblasts.

Preliminary experiments showed that the tested OR sequences were enriched for H3K9me3 and H4K20me3 in the MOE, whereas in the other cell types, there was significant enrichment only for H3K9me2 (data not shown).

To examine the distribution of the two heterochromatic marks on all ORs, we performed ChIP-on-chip experiments using Nimblegen whole-genome tiling arrays with immunoprecipitated DNA from MOE and liver. We found that most ORs are hypermethylated on H3K9 and H4K20 in the MOE, but not in the liver. The distribution of the two modifications along chromosomes 2, 7, and 9, which contain large OR genomic clusters, is depicted as heatmaps in Figure 1A, where genes are ordered by chromosomal position. Most genes, independently of their transcription status, appear to be devoid of both modifications in both tissues. However, in the MOE, there is significant enrichment for H3K9me3 and H4K20me3 on ORs. The high enrichment for the two modifications combined with the tandem chromosomal organization of these genes highlights the position of each OR cluster in these three chromosomes (Figure 1A). Vomeronasal receptor (VR) genes, which encode monoallelically expressed receptors that detect pheromones (Dulac and Axel, 1995), are also enriched for H3K9me3 and H4K20me3 in the MOE (Figure 1A, chromosome 7). ORs and VRs are hypomethylated in the liver, in agreement with published observations that report the complete absence or the low abundance of these marks on OR genes in numerous cell types (Celniker et al., 2009; Hawkins et al., 2010; Larson and Yuan, 2010).

A Heterochromatic Signature for Chemoreceptors

To obtain a global view of our ChIP-on-chip data, we ranked the mouse genes based on the average signal intensity of H3K9me3 and H4K20me3 over a region of 2Kb (Figures 1B and 1C), using the translational start site (TSS) as a coordinate for the alignment of the mouse genes. To present the data in a visually comprehensive manner, we included only every 15th mouse gene in the presentation, although the analysis was performed for all of the genes. In Figure 1B, 1000 randomly selected genes are ranked in descending order by their enrichment values for the two modifications. OR genes, depicted by blue lines at the side of the heatmap, are clustered on the very top, showing that they are the most enriched genes for H3K9me3 and H4K20me3 in the MOE. In a zoomed-in view of the top 1000 genes (Figure 1C), OR genes constitute the majority of genes with significant enrichment for both trimethyl marks ($p < 10^{-7}$). Sequential ChIPs with chromatin from the MOE confirmed the simultaneous presence of these marks on OR chromatin (Figure S1A available online). Notably, as shown also in Figure 1A, the evolutionary older type I OR genes that are organized in a unique cluster on

(A) Positional heatmaps of chromosomes 2, 7, and 9 are shown. Each row represents one gene in 1 kb windows from −5 kb to +5 kb of the TSS. Four states are shown as adjacent columns: liver-H3K9me3, OE-H3K9me3, liver-H4K20me3, and OE-H4K20me3. Arrows indicate OR, V1R, and V2R clusters found on these chromosomes.

(B) Ranked heatmap illustrating 1000 randomly selected genes (∼1 in 15 genes). Each row represents one gene in 200 bp windows from −1 kb to +1 kb of the translation start site. The ORs (blue lines) make up the vast majority of the genes that are positive for both modifications and are placed at the top of the heatmap. The red lines represent VRs and FPRs.

(C) Ranked heatmap, constructed as the previous one but showing the top 1000 genes that are positive for H3K9me3 and H4K20me3 in the MOE. Most of these genes are ORs that also rank the highest, as depicted by the blue lines next to the heatmap.
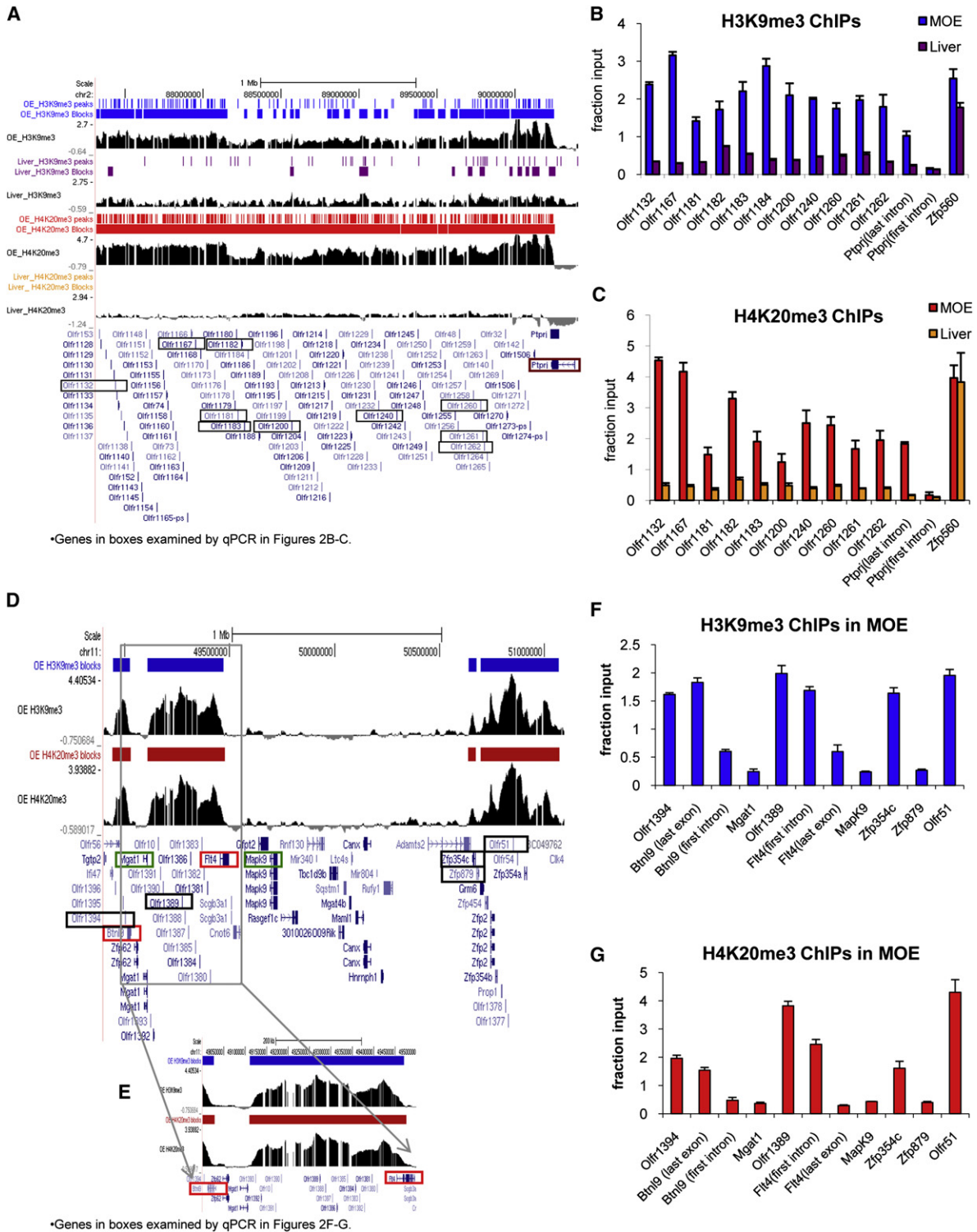
See also Figure S1.

Figure 2. OR Clusters in the MOE Are Coated by Tissue-Specific Heterochromatic Blocks of H3K9me3 and H4K20me3

Ma2C analysis of our ChIP-on-chip data viewed on the UCSC genome browser.

(A) Part of the biggest OR cluster located on chromosome 2, which contains ~240 genes and spans a 5 MB region. The thin blue (H3K9me3) or red (H4K20me3) bars represent significant peaks (FDR $\leq$ 5%) identified in the MOE by MA2C using standard parameters (window = 0.5 kb, min number of probes = 5, max gap = 0.25 kb); the thick blue or red bars represent the blocks identified with modified parameters (window = 10 kb, min number of probes = 20, max gap = 1 kb). In the liver, there are only a few sporadic H3K9me3 peaks and blocks (purple).

chromosome 7 have the lowest enrichment values among ORs. Most of the non-OR genes that are enriched for H3K9me3 and H4K20me3, represented by red lines in Figures 1B and 1C, are also chemoreceptors, namely VRs and formyl-peptide receptors (FPRs), which are also clustered in extremely AT-rich isochores and likely follow the same regulatory logic as ORs (Figures S1B and S1C) (Dulac and Axel, 1995; Liberles et al., 2009; Rivière et al., 2009). Unlike chemoreceptors, the KRAB-ZFP genes are heterochromatinized also in the liver and in other cell types (Barski et al., 2007; O'Geen et al., 2007).

Heterochromatic Macrodomains Cover the OR Clusters in the MOE

To identify significant sites of enrichment within OR clusters, we used the Ma2C algorithm (Song et al., 2007). Using a sliding window of 0.5 Kb and FDR $\leq$ 5%, we observed that, in the MOE, the peaks for the two histone modifications were contained in broadly enriched genomic regions spreading throughout the OR clusters in an almost continuous arrangement (Figure 2A). Modification of the Ma2C parameters so that local signal fluctuations would be averaged over a larger sliding window of 10 Kb confirmed that H3K9me3 and H4K20me3 form heterochromatic macrodomains (blocks) that cover megabases of clustered OR genes in the MOE (Figure 2A). Using this analysis, we found that 1376 ORs fall in H4K20me3 blocks and 1109 ORs fall in H3K9me3 blocks, out of a total of 1441 annotated OR genes (Figure S1D) (p < 10^{-7}). The presence of heterochromatic macrodomains over OR clusters was also confirmed by the application of an independent algorithm that was developed and used for the detection of long stretches of H3K9me2 in the liver, brain, and ES cells (Figures S2A and S2B) (Wen et al., 2009). In contrast to our findings in the MOE, there are only few H3K9me3 and H4K20me3 peaks and blocks on the ORs in the liver (Figure 2A) that do not overlap and are not confirmed by qPCR (see below). As an independent estimate of the H3K9me3 and H4K20me3 enrichment on OR loci in the two tissues, we combined multiple ChIPs and analyzed them by Southern blot. As a probe, we used a ~600 bp reverse transcriptase-polymerase chain reaction (RT-PCR) product, generated by a degenerate primer pair, which contains several hundred OR sequences (Buck and Axel, 1991). As seen in Figure S2C, the OR hybridization signal of the H3K9me3 and H4K20me3 ChIPs from the MOE is significantly higher than the signal in the liver. We further

validated our ChIP-on-chip and ChIP-Southern results by ChIP-qPCR for multiple OR gene clusters in both tissues. Representative data are shown in Figures 2B and 2C and Figures S2E and S2F. Interestingly, the external borders of the heterochromatic blocks coating the OR clusters coincide with the borders of the OR genomic loci (Figures 2A and 2D). The reported binding of CTCF outside of OR clusters (Kim et al., 2007), or other insulating elements (Dickson et al., 2010), might contribute to the confinement of OR heterochromatin within the OR clusters.

In few instances, embedding transcriptionally active non-OR genes in an OR cluster interrupts the heterochromatin blocks until the presence of another OR reconstitutes them (Figures 2D-2G). In contrast, genes that are not transcribed in the MOE are partially covered by heterochromatin marks, suggesting that, in the absence of a competing transcriptional state or an insulating activity, the OR heterochromatin can extend to the body of non-OR genes within an OR cluster.

Characterization of the OR Heterochromatin

Our data demonstrate that OR clusters in the MOE fall in silent domains marked by H3K9me3 and H4K20me3, whereas, in the liver, they are enriched only for H3K9me2. To determine whether there are functional differences stemming from these chromatin modifications, we treated nuclei from MOE and liver with DNase I and examined the accessibility of different loci by qPCR analysis of the recovered DNA. As seen in Figure 3A and Figures S3A and S3B, there is significant difference in DNase I sensitivity of ORs between the two tissues. In MOE, OR genes get hardly digested, even after 40 min of incubation with DNase I, suggesting an inaccessible chromatin structure. In contrast, transcriptionally active genes are rapidly digested, and silent non-OR genes have intermediate accessibility properties. In liver, OR loci are indistinguishable from other genes regarding their DNase I accessibility (Figure 3A). The DNase I-qPCR data were also confirmed by a different method. DNA with similar size distribution, extracted from DNase treated nuclei from MOE and liver, was subjected to Southern blot analysis using the degenerate OR probe described earlier. As seen in Figure S3C, hybridization signal intensity is stronger in the MOE than in the liver, but most importantly, the signal in the MOE is concentrated to the larger DNA fragments, providing additional evidence that OR chromatin is less accessible in the MOE. Hybridization of the same membrane with a ribosomal

---

(B) Results from H3K9me3 ChIP-qPCR analysis using native chromatin preparations from MOE and liver. The *Ptprj* gene (marked by red rectangle in 2A) stands at the border of the OR cluster, which coincides with the border of the heterochromatic block. Its most proximal—to the OR cluster—intron is enriched for H3K9me3 and H4K20me3, and its most distal intron, located 43 kb downstream, is free of these modifications. *Zfp560* serves as positive control.

(C) Same as (B) but for H4K20me3.

(D) Part of an OR cluster on chromosome 11 is interrupted by a small group of non-OR. Genes that are marked by a green rectangle are transcriptionally active in the MOE, and genes marked by red rectangles do not have detectable transcripts.

(E) Zoomed-in picture of the cluster, which shows that genes *Btnl9* and *Flt4*, which are transcriptionally inactive, are partly methylated. Two sets of primers for each of these genes, one at the beginning (most proximal to the neighboring OR gene) and one at the end of the gene (most distal from the neighboring OR), were used in ChIP-qPCR.

(F) Results from H3K9me3 ChIP-qPCR analysis using native chromatin preparations from the MOE. OR genes tested, as well as *Zfp354c*, and part of the *Btnl9* and *Flt4* genes were enriched. In contrast, the active genes *Mgat1* and *Mapk9*, *Zfp879*, and the distal part of *Btnl9* and *Flt4* were devoid of modifications.

(G) Same as (F) but for H4K20me3.

All above experiments were performed in two biological replicates with similar results. Values are the mean of triplicate qPCR. Error bars indicate the SEM. See also Figure S2.
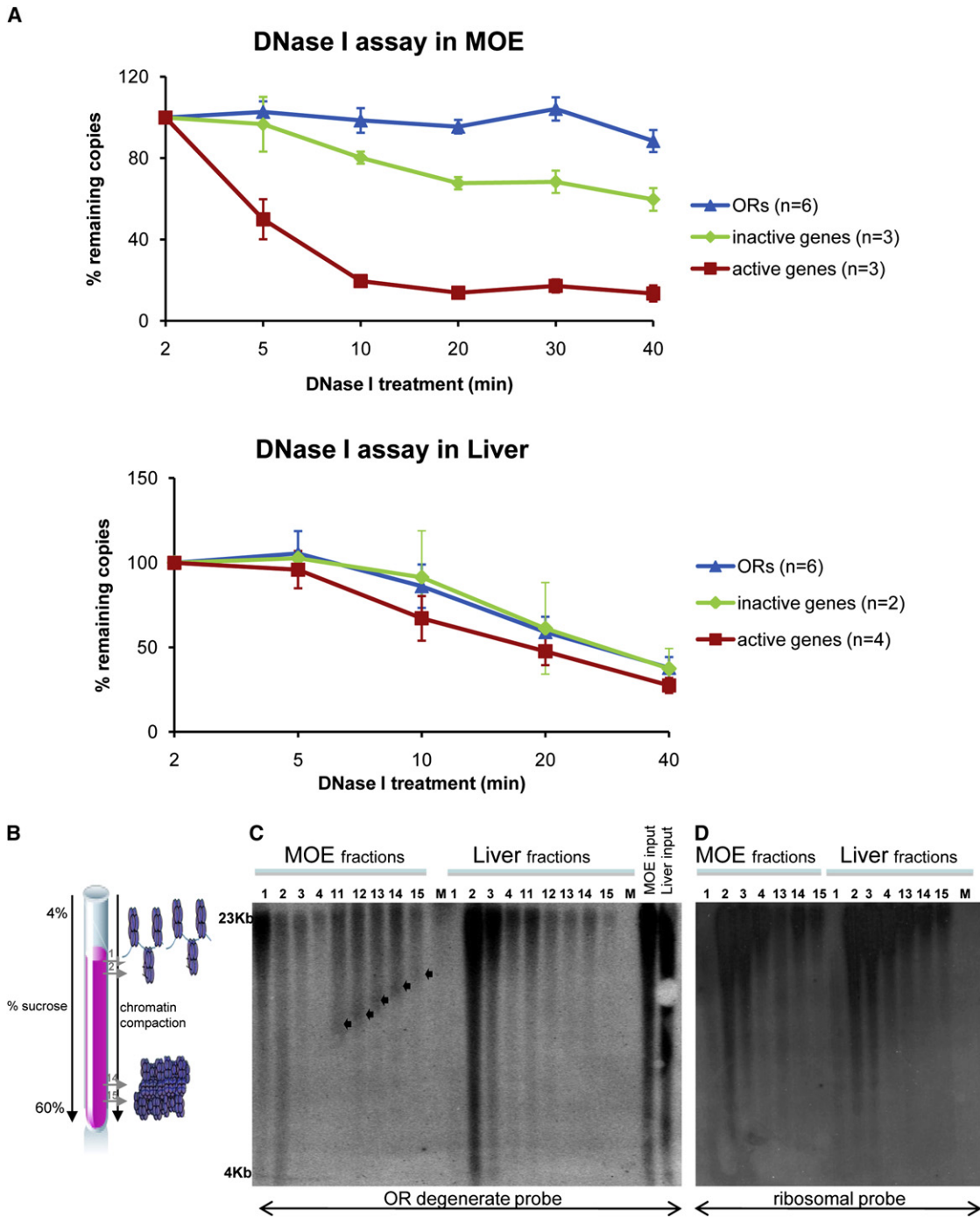
Figure 3. The ORs Acquire a Highly Compacted Chromatin Structure in the MOE

(A) DNase I accessibility assay with nuclei from both MOE and liver. Nuclei were treated with DNase I, DNA was isolated at various time points (2–40 min), and equal amounts were used for qPCR. The amount of DNA measured at each interval was expressed as a fraction of the DNA present at 2 min of enzyme treatment and was plotted over time. We assayed several ORs as well as genes that are active or inactive in the MOE or liver, and their mean is shown here (see Figures S3A and S3B for detailed analysis of all genes). Representative data from one experiment are shown here.

(B) MNase-digested chromatin was submitted to ultracentrifugation through a sucrose gradient. The largest or most compacted chromatin fragments are collected in the fractions with the highest sucrose concentration. For a particular fragment size, the most compact chromatin is collected in more concentrated fractions.

(C) Fractions from MOE and liver analyzed by agarose gel electrophoresis and Southern blot with a degenerate OR probe. Arrows mark the low-molecular weight OR sequences that appear in the bottom fractions of the chromatin from the MOE. Input lanes represent DNA extracted from chromatin that was not loaded in the gradient.

(D) Selected fractions from the same experiment analyzed with the use of a ribosomal probe.

See also Figure S3.

probe shows that the digestion differences do not reflect universal differences between the two tissues.

To test directly the idea that OR heterochromatin has a more compacted chromatin arrangement in the MOE, we examined the buoyancy properties of OR chromatin (Ghirlando et al., 2004; Gilbert et al., 2004). We performed limited MNase digestion of MOE and liver chromatin followed by ultracentrifugation in sucrose gradient (4%–60%) (Figure 3B). MNase digests native chromatin independently of the compaction levels or the transcriptional state of each locus (Weintraub and Groudine, 1976). Thus, digestion with MNase produces chromatin fragments of similar length distribution in the two tissues (Figure 3C). Chromatin fractions were collected from top to bottom, and the DNA was analyzed by gel electrophoresis and Southern blot. Figure 3C shows that the distribution of OR DNA is dramatically different across fractions from the two tissues. In the liver preparation, the strongest OR signal appears in the second and third fractions. In contrast, in the MOE, there is OR DNA in the first fractions but also a substantial signal in the bottom five fractions (depicted by arrows). Importantly, the signal in the fractions that correspond to the highest sucrose concentration comes from OR DNA of lower molecular weight, consistently with highly compacted chromatin. Selected fractions from the same preparation analyzed by a ribosomal probe verified the specificity of OR chromatin compaction in the MOE (Figure 3D).

OR Silencing Is Independent of OR Expression

The MOE is a heterogeneous tissue composed of multiple cell types (Duggan and Ngai, 2007) (Figure S4A). Although OSNs comprise the majority of cells in our dissections, we sought to confirm that our findings describe the chromatin state of OR genes in the OR-expressing neurons. For this reason, we performed a series of fluorescence-activated cell sorting (FACS) experiments followed by ChIP-qPCR.

We isolated mature OSNs from OMP-IRES-GFP mice (Figure 4A), and as seen in Figure 4B, the OR genes tested have high levels of enrichment for both H3K9me3 and H4K20me3 in these cells. Although mature OSNs express ORs, each OR gene is expressed in 0.1% of the cells; thus, it is not surprising that we detect silencing marks on them. The confirmation, however, that ORs are heterochromatinized in OSNs raises questions of whether this silencing is induced by OR expression as a consequence of the feedback signal. To address this, we sorted sustentacular cells from the MOE with the use of SUS4 antibody (Chen et al., 2004). Sustentacular cells line the apical surface of the epithelium (Figure 4C) and have common developmental ancestors with the OSNs, but they do not express ORs (Figure 4H). Figure 4D shows that, in sustentacular cells, the levels of H3K9me3 and H4K20me3 on ORs are comparable to the levels of these marks in mature OSNs, suggesting that marking of OR genes with H3K9me3 and H4K20me3 occurs in the absence of OR expression. In this scenario, it is possible that trimethylation of lysines 9 and 20 takes place before OR activation.

To explore this possibility, we performed ChIP-qPCR analysis in progenitor cells, starting with the most multipotent cells of the MOE, the horizontal basal cells (HBCs) (Leung et al., 2007), by sorting ICAM-1$^+$ cells (Carter et al., 2004) (Figure 4E). As seen in Figure 4F, there is no enrichment for H3K9me3 and H4K20me3 on OR genes, whereas the pericentromeric repeats and the KRAB-ZFP genes (Zfp560) are already hypermethylated. Interestingly, we detect high signal for H3K9me2 on ORs in the HBCs (Figure S4B), showing that, in this multipotent state, ORs are repressed via different mechanisms.

We also examined the chromatin state of OR genes in other progenitor cells from the MOE that are negative for OMP, ICAM-1, immature laminin receptor (iLR) (another marker for multipotent basal cells [Jang et al., 2007]), and SUS4. As seen in Figure 4G, in this population, the enrichment for H3K9me3 and H4K20me3 on the tested ORs is as high as in the OMP$^+$ cells. This quadruple-negative population does not express ORs at levels that are detectable by RT-PCR (Figure 4H). The above data suggest that trimethylation of ORs occurs at a stage preceding OR expression.

To examine a better-defined progenitor cell population, we obtained a Neurogenin1-GFP (Ngn1-GFP) BAC transgenic reporter mouse from GENSAT (Heintz, 2004). As expected, GFP$^+$ cells appear in the basal layer of the MOE in sections of this strain (Figures 5A and 5B), consistent with the reported expression of Ngn1 (Cau et al., 2002). RT-PCR analysis showed that these cells represent a mixed population of progenitors and immature neurons (Figure S5A). Immunofluorescence with anti-MOR28, M50, and M71 antibodies (Barnea et al., 2004) in sections of the transgenic mice verified the mutually exclusive expression of ORs and Ngn1 (Figures 5A and 5B). However, for a more sensitive and global view of the levels of OR transcription in the Ngn1$^+$ cells, we performed deep sequencing with cDNA from Ngn1$^+$ and OMP$^+$ cells (see Table S1). We detected transcripts for 1185 OR genes in the mature OSNs with an average of 8-fold higher mRNA levels than in the Ngn1$^+$ cells (Figures 5C and 5D). Importantly, in the Ngn1$^+$ cells, ~95% of OR genes have transcript levels similar to the transcript levels of silent genes (data not shown). The low levels of OR mRNA in these cells probably reflect a small percentage of contaminating mature OSNs, detected by the extreme sensitivity of RNaseq. In agreement, 25 genes that constitute markers of mature OSNs (Sammeta et al., 2007) are also detected in low levels in the Ngn1 sample, at a similar 7-fold average reduction.

FACS and ChIP-qPCR analysis of the Ngn1$^+$ cells revealed high levels of enrichment for H3K9me3 and H4K20me3 on ORs, demonstrating similar heterochromatic signature with the mature OSNs (Figure 5E). Had only the few OR-expressing cells contributed the H3K9me3 and H4K20me3 signal on OR genes, the trimethylation signal would have also been 8-fold lower in the Ngn1$^+$ cells. Therefore, the ChIP-qPCR data from the quadruple-negative cells and Ngn1$^+$ cells are consistent with H3K9me3 and H4K20me3 having been deposited on OR genes before OR expression.

To test the consequences of the transition of di- to trimethylation in the chromatin structure of ORs, during MOE differentiation, we performed the same DNase I-Southern blot analysis described earlier, using FAC sorted ICAM1$^+$, Ngn1$^+$, and OMP$^+$ cells. Figure 5F demonstrates that the differentiation of HBCs to Ngn1$^+$ cells coincides with increased protection from
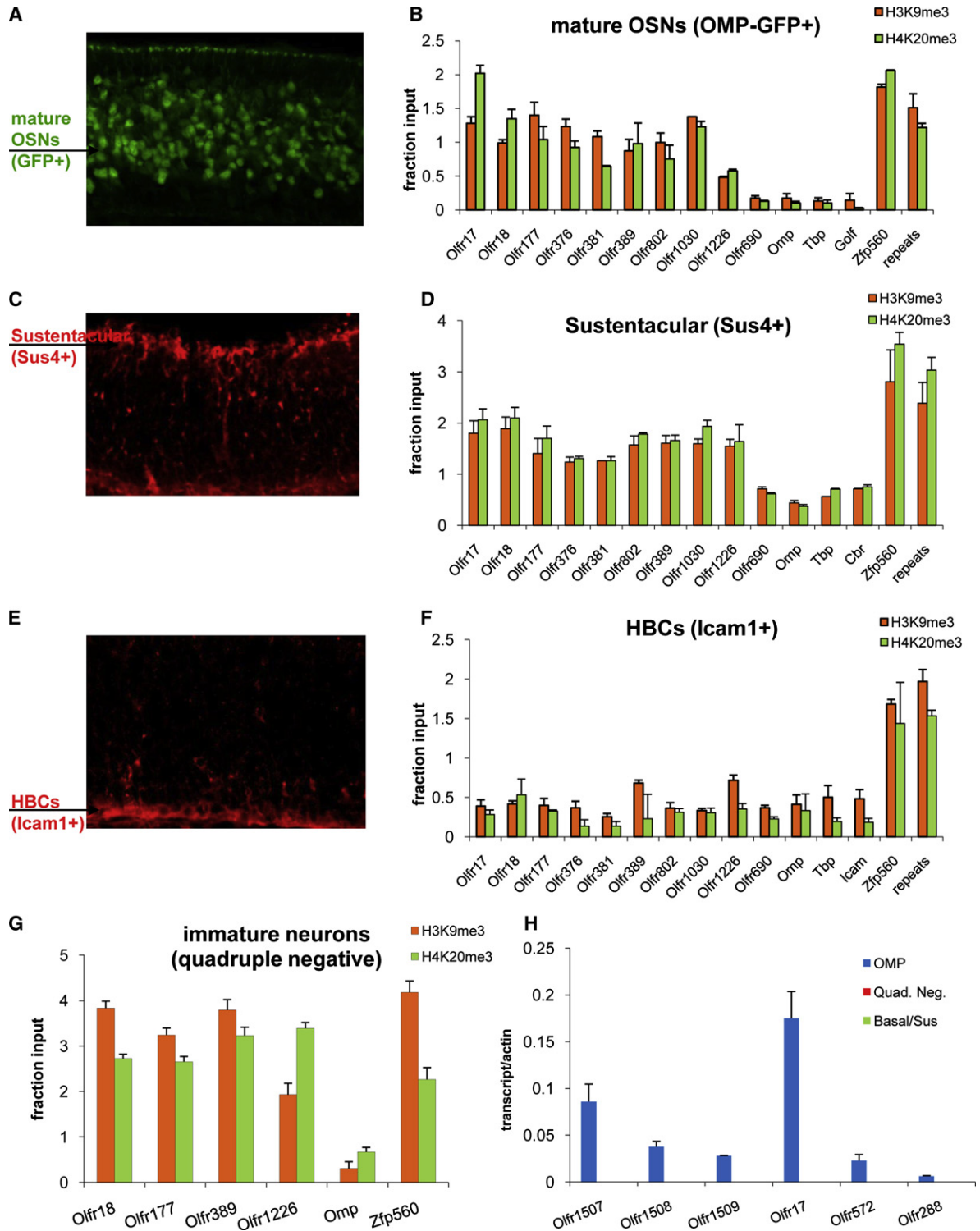
Figure 4. ChIP-qPCR Assays for H3K9me3 and H4K20me3 in Sorted Cell Populations from the MOE

(A) Section of the MOE from an adult OMP-IRES-GFP mouse. Mature OSNs are GFP[+].

(B) GFP^{+} cells (mature OSNs) were isolated with FACS from OMP-IRES-GFP mice and were used for ChIP-qPCR experiments. *Golf*, *Tbp*, and *Omp* are active genes in these cells and are used as negative controls. *Zfp560* and major satellite repeats are used as positive controls. *Olfr690* is a type I OR.

(C) Immunostaining of MOE section with SUS4 antibody that specifically labels the sustentacular cells.

(D) ChIP-qPCR with isolated sustentacular cells. *Cbr* is an active gene and is used as a negative control.

DNase I digestion, suggesting that this epigenetic transition results in a less accessible OR chromatin structure retained in mature OSNs.

An "Epigenetic" Switch Accompanies OR Choice

To test whether the active OR allele is free of H3K9me3/H4K20me3, we enriched, by FACS, for neurons expressing the olfactory receptor P2 from P2-IRES-GFP knocked in mice. We isolated ~40,000 GFP$^+$ and GFP$^-$ neurons from P2-IRES-GFP heterozygote mice and performed ChIP-qPCR for H3K9me3 and H4K20me3. To monitor specifically the active allele, we used a primer pair for GFP, which follows the epigenetic properties of the P2 locus (data not shown), and a primer pair specific for the wild-type P2 (p2WT) to monitor the inactive allele (Figure 6A). As seen in Figures 6B, 6C, and 6F, the enrichment for H3K9me3 and H4K20me3 is significantly reduced on the active OR allele, compared to the enrichment of the inactive allele or the enrichment of the same sequence in the GFP$^-$ population. *Olfr177*, which is expressed in a different zone than *P2*, is also highly enriched for H3K9me3 and H4K20me3, suggesting that the primary function of this silencing mechanism is not the restriction of OR expression within a zone. Notably, the levels of H3K9me3 and H4K20me3 on the active allele are reduced, but not eliminated. Control experiments in which the GFP$^+$ population was checked for purity indicated that there was ~30% contamination, a result that was expected because we were sorting for an extremely rare population (~0.05% of total cells in the MOE). To obtain a pure population, we performed a double FACS experiment; the GFP$^+$ cells were sorted again, resulting in a > 95% GFP$^+$ population. For this experiment, we used MOR28-IRES-GFP heterozygote knockin mice, which provide more GFP$^+$ cells than the P2-IRES-GFP mice. As seen in Figures 6D and 6E, ChIP-qPCRs from this extremely pure population provide strong evidence that H3K9me3 is absent from the transcriptionally active *MOR28* allele.

To further examine the epigenetic state of the active allele, we performed ChIP-qPCR in P2-expressing neurons using an antibody against H3K4me3, which is found on active and poised promoters (Guenther et al., 2007) and has a mutually exclusive distribution with H3K9me3 and H4K20me3 (Regha et al., 2007). In agreement with this incompatibility, H3K4me3 cannot be detected on OR promoters using chromatin preparations from the whole MOE (data not shown). As seen in Figure 6G, only in the GFP$^+$ population is there high enrichment for H3K4me3 on the P2 promoter and CDS, supporting the idea that activation of the *P2* allele correlates with the removal of H3K9me3 and H4K20me3. Although H3K4me3 is very abundant throughout the active *P2* allele, it is missing from the neighboring *P3* and *P4* genes (Figure 6G and Figures S6A and S6B), despite

the sequence similarity between these genes and their expression in the same zone. Expression analysis of P2-GFP$^+$ cells confirmed the enrichment for P2-expressing neurons (Figure S6C).

Heterochromatic Marks Induce Silencing and OR-like Expression

Our data suggest that heterochromatinization of OR loci prevents the simultaneous expression of every OR gene in every OSN. To test whether this heterochromatic structure can influence gene expression, we examined a transgenic mouse, in which an OMP promoter-driven LacZ transgene had been inserted proximal to a singular OR gene (*Olfr459*). Unlike numerous OMP-LacZ- or OMP-GFP-independent transgenes that are expressed in the majority of olfactory neurons (Nguyen et al., 2007; Walters et al., 1996), this transgene is silent in 99.9% of the neurons and has a sporadic and mostly zonal expression reminiscent of that of the neighboring *OR* (Pyrski et al., 2001).

We reasoned that this transgene is inserted within the heterochromatic block flanking *Olfr459*. Unlike non-OR genes located in OR clusters, which probably developed insulating mechanisms that prevented heterochromatic silencing (e.g., *Mgat1* in Figure 2D), transgenes are influenced by the local chromatin architecture. Mapping the exact insertion site of this transgene revealed that it resides ~55 kbs from *Olfr459* (Figure 7A). ChIP-qPCR experiments showed that the insertion site is heterochromatinized in wild-type mice and remained so after the transgenic insertion (Figures 7B and 7C). ChIP-qPCR on chromatin prepared from the transgenic mice confirms that this reporter is marked by H3K9me3/H4K20me3 in an MOE-dependent fashion, in contrast to the endogenous OMP promoter, which is unmethylated (Figure 7C).

To examine whether the insertion of the OMP transgene within OR-heterochromatin also results in monoallelic expression, we compared the number of β-gal$^+$ cells between homo- and heterozygous mice. As seen in Figure 7D, OMP-LacZ homozygotes have in average 1.8-fold more β-gal$^+$ cells, consistent with a monoallelic expression pattern that clearly does not stem from the promoter properties of OMP. Finally, to test whether this reporter is under the transcriptional control of the OR locus, as indicated by the epigenetic influence of the locus, we crossed this transgenic mouse with the Emx2 knockout mice (Pellegrini et al., 1996). Emx2 is required for the expression of *Olfr459* and most OR genes, but it does not have significant effects on OMP expression (McIntyre et al., 2008). Figure S7 shows that the reporter expression is abolished in the Emx2 KO mice, suggesting that this transgene conforms to the regulatory logic of the neighboring OR.


(E) Immunostaining of MOE section with an antibody against ICAM-1 (PE-ICAM-1) that specifically labels the HBCs.

(F) ChIP-qPCR experiments with isolated HBCs.

(G) ChIP-qPCR with immature neurons and progenitors from the MOE isolated by collecting OMP$^-$, ICAM$^-$, iLR$^-$, and Sus4$^-$ cells (quadruple negative).

(H) RNA isolated from combined OMP-GFP$^+$, sustentacular, and basal cells or quadruple-negative cells was used in qRT-PCR reactions with primers for different ORs. Actin was used as endogenous control.

All above experiments were performed in at least two biological replicates with similar results. Values shown here are the mean of triplicate qPCRs. Error bars represent the SEM. See also Figure S4.
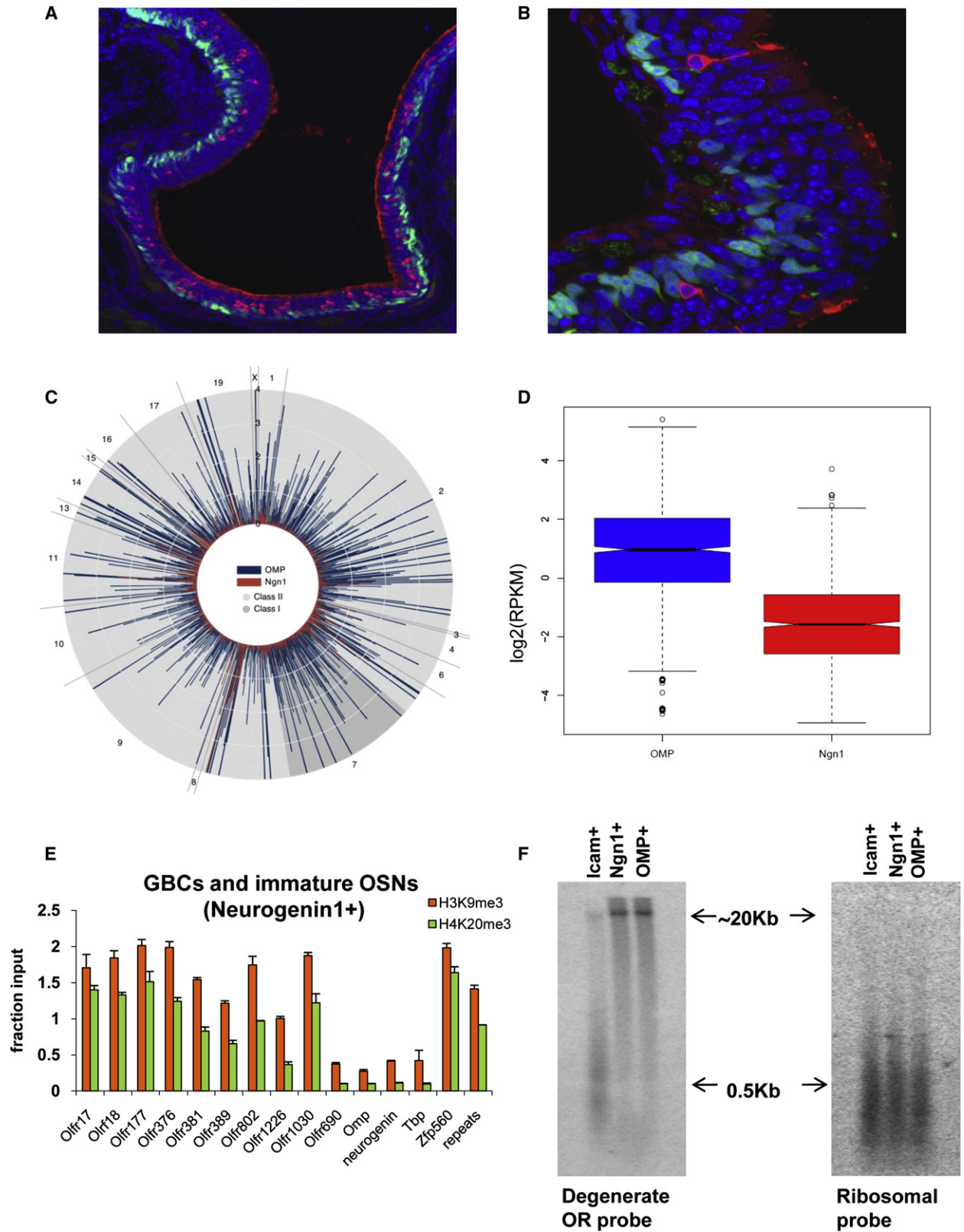
DISCUSSION

OR choice is a seemingly stochastic process that culminates in the expression of one out of ~2800 OR alleles under poorly understood molecular mechanisms. Here, we show that the hallmarks of constitutive heterochromatin, H3K9me3 and H4K20me3, are deposited on OR loci in the MOE. The extensive marking of OR genes by these methyl groups results in the generation of compacted heterochromatic macrodomains that are likely incompatible with transcription. In agreement with an instructive role of this chromatin structure in gene expression, insertion of an OMP-LacZ transgene in OR heterochromatin results in the transcriptional silencing of this reporter in ~99.9% of the OSNs, leading to an OR-like, sporadic, and likely monoallelic expression.

The genome-wide ChIP-on-chip analysis presented here provides a rare example for the involvement of H3K9 and H4K20 trimethylation in transcriptional choices in addition to their function in telomeric and pericentromeric silencing. Consistent with a role in OR regulation, H3K9me3 and H4K20me3 mark OR genes in the MOE in a developmentally regulated fashion. They are added to the—already repressed via H3K9me2—OR chromatin during the transition from HBCs to immature OSNs and are possibly removed later from a single OR allele with remarkable precision, as the neighboring ORs remain heterochromatinized. Therefore, our data describe an unusual form of silencing that combines characteristics of both constitutive and facultative heterochromatin; OR heterochromatin has the same molecular and biochemical characteristics as the pericentromeric and telomeric heterochromatin, but it is dynamic and it depends on the identity of the cell and its differentiation state.

Different Repressive Methyl Marks Induce Distinct Chromatin Properties

The finding that ORs are kept inactive in most tissues examined via H3K9 dimethylation poses questions regarding the requirement for H3K9 and H4K20 trimethylation in the MOE. The observation that the additional lysine methylation events result in less accessible chromatin structure, which likely prevents the binding of OR-activating and OSN-specific transcription factors on multiple OR alleles, offers a simple explanation. In other words, this transition in methyl marks provides better protection from the activating transcription factor millieux and more efficient

repression, offering a unique and counterintuitive example in developmental biology whereby genes are silenced in the exact cell type that they are supposed to be expressed, assuring the implementation of the "one receptor per neuron rule." Indeed, ChIP-qPCR from P2-expressing neurons shows that the primary function of this silencing mechanism extends beyond the restriction of OR expression within a zone because, in a P2-expressing neuron, genes from the same or different zones have similar trimethylation levels.

OR Silencing Precedes OR Choice

Our data suggest a model for OR choice that incorporates our biochemical findings with a feedback signal. According to this model, all of the OR alleles become silenced before OR transcription. At a later stage, a limited enzymatic activity removes H3K9me3 and H4K20me3 from a stochastically chosen allele, allowing its transcriptional activation. The synthesis of OR protein elicits a feedback signal that prevents this enzyme/selector from activating another allele and stabilizes the transcription of the chosen allele. Thus, the feedback signal does not silence the nonchosen OR alleles but prevents their desilencing. Consequently, an OR-generated feedback is not responsible for creating the singularity in OR choice but, rather, for preserving it for the life of the neuron.

Alternatively, at the moment of OR choice, OR genes could be repressed only by H3K9me2, which is deposited on them at earlier differentiation states. In this scenario, OR expression could trigger the trimethylation of H3K9 and H4K20, resulting in permanent OR silencing. However, our data are consistent with the former model. We detect high levels of H3K9me3 and H4K20me3 on sustentacular cells that do not express ORs and do not experience such a feedback. Second, we isolated progenitor cells and immature OSNs and progenitors with two independent approaches, and in both cases, OR silencing was detected before OR expression. In any case, the molecular logic of OR choice is conceptually the same: in both models, chromatin-mediated silencing precedes OR choice. Finally, it is plausible that OR choice constitutes the "protection" of one OR allele from either form of silencing. However, it is established that OSNs can switch to different OR alleles (Shykind et al., 2004), making such a model highly unlikely.

Our data cannot exclude the possibility that trimethylation of H3K9 and H4K20 constitutes epi-phenomena causing neither

---

Figure 5. Expression and ChIP-qPCR Analysis of Ngn1^{+} Cells

(A and B) Sections of the MOE from an adult Ngn1-GFP mouse stained with antibodies against ORs MOR28 and M50 (A) or M71 (B) (all in red). GBCs and immature neurons are the GFP^{+} cells (green).
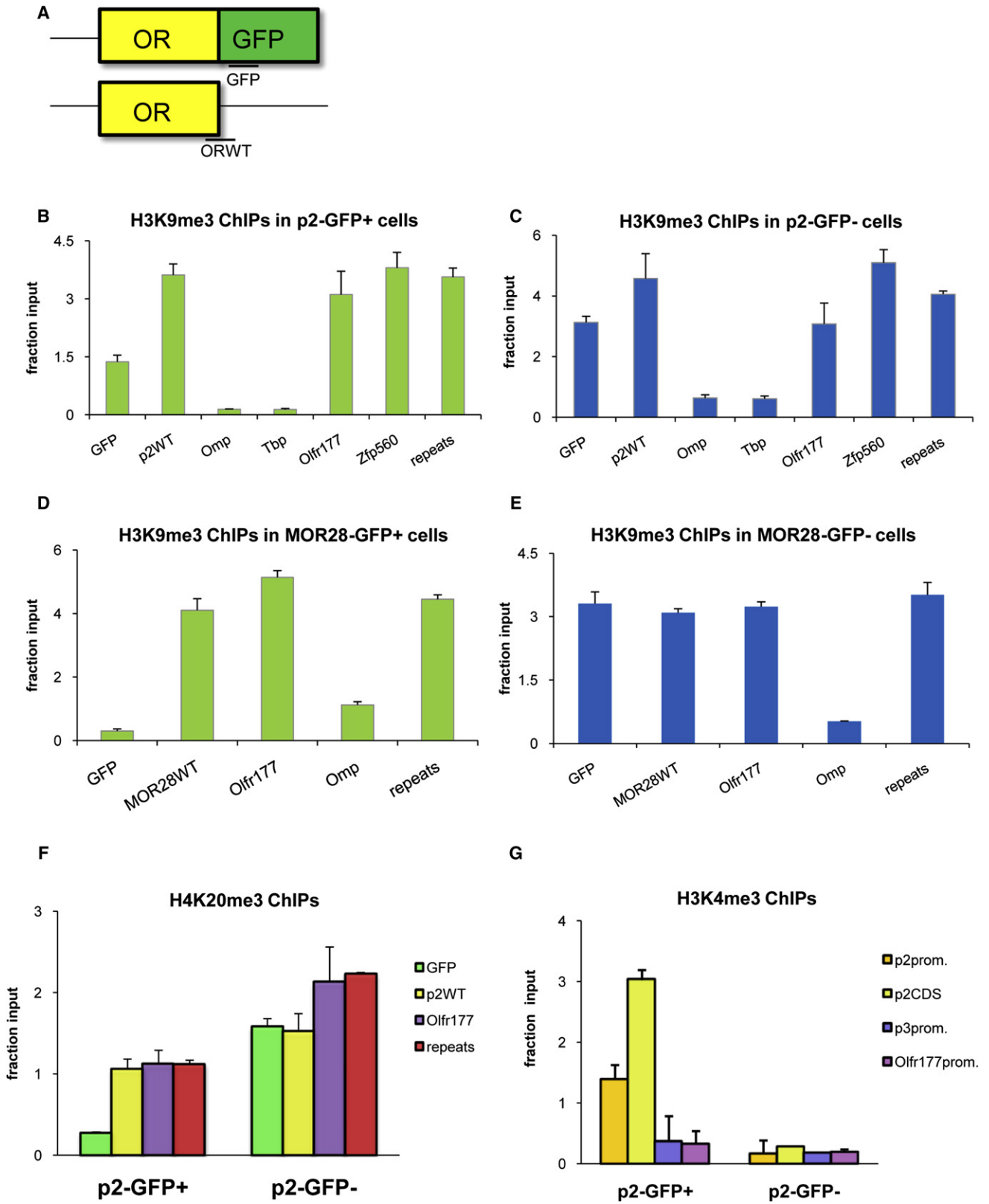
(C) Expression levels of OR transcripts, as determined by Illumina mRNA-seq, are quantified by normalized RPKM (reads per kilobase of exon model per million mapped reads). RPKM increases with radius from the center of the figure, clamped at a maximum of 1. Each radial bar represents the level of expression of a single OR. For each OR gene, red indicates the expression level in Ngn1^{+} neurons, and blue indicates the expression level in OMP^{+} neurons. ORs are sorted first by chromosome, indicated by the number or letter exterior to each wedge of the figure, and then by increasing gene start position within each chromosome. The two classes of ORs (classes I and II) are demarcated by background shading. See Table S1 for detailed results.

(D) Boxplot representation of all OR gene expression in OMP[+] and Ngn1^{+} cells, showing that there is an ~8-fold difference between the two cell types. Per gene expression was calculated in log2 (RPKM) units.

(E) ChIP-qPCR analysis for H3K9me3 and H4K20me3 with isolated Ngn1-GFP^{+} cells. Experiment was performed in two biological replicates with similar results. Values shown here are the mean of triplicate qPCRs. Error bars represent the SEM.

(F) ICAM-1^{+}, Ngn1^{+}, and OMP^{+} cells were sorted from the MOE of adult mice, and their nuclei were extracted, digested with DNase I, and analyzed by agarose gel electrophoresis and Southern blot with a degenerate OR or a ribosomal probe.

See also Figure S5.

A

B H3K9me3 ChIPs in p2-GFP+ cells

C H3K9me3 ChIPs in p2-GFP- cells

D H3K9me3 ChIPs in MOR28-GFP+ cells

E H3K9me3 ChIPs in MOR28-GFP- cells

F H4K20me3 ChIPs

G H3K4me3 ChIPs

the chromatin compaction nor the transcriptional silencing of OR genes. However, there is significant support from multiple model organisms for a direct role of these epigenetic modifications in chromatin structure and gene regulation (Fodor et al., 2010).

In conclusion, our experiments provide a molecular glimpse into the monoallelic expression of olfactory receptors in the mouse. In the other well-characterized stochastic regulatory process in mammals, X inactivation, the choice is made between two transcriptionally active X chromosomes; whereas one will remain on, the other will be silenced as a consequence of the choice (Royce-Tolland and Panning, 2008). In OR choice, the logic is different. Silencing occurs before a choice is made, and the choice itself could be mediated by derepression. Similar logic applies to the immunoglobulin light chain rearrangement and to *var* gene choice in *Plasmodium falciparum* (Goldmit et al., 2005; Scherf et al., 2008). A common theme between OR, kappa, and *var* gene choice is the high number of available alleles (Goldmit and Bergman, 2004). If these genes were maintained in a poised and accessible state, then the concomitant selection of multiple alleles would be unavoidable. Therefore, the high number of OR alleles together with the need for a strictly monogenic and monoallelic OR expression gave rise to an unusual regulatory circuit. It remains to be seen whether the regulatory principles proposed here apply to other neuronal systems whereby neurons commit permanently to differentiation processes regulated by stable transcriptional choices.

EXPERIMENTAL PROCEDURES

Animal Care
Mice were treated in compliance with the rules and regulations of IACUC under a protocol approval number AN084169-01.

ChIP-qPCRs and ChIP-on-Chip Experiments
ChIP-qPCRs assays, sequential ChIPs, and ChIP-on-chip experiments were performed according to standard protocols and are described in detail in Extended Experimental Procedures.

Data Analysis
Quality control of the ChIP-on chip data was performed both by NimbleGen (according to their protocols) and by our group. The log2 (ChIP/input) ratio was normalized in a "weighted global" manner. For peak analysis, we used the model-based analysis of two-color arrays (MA2C) (Song et al., 2007), which is a variation of the general sliding window approach. We also confirmed our results by a different algorithm (Wen et al., 2009). See Extended Experi-

mental Procedures for more details. Raw and normalized Chip-on-chip data can be accessed at GEO: GSE24420.

DNase I Accessibility Assay
Nuclei were isolated from MOE and liver and digested with DNase I for 2–40 min at 37°C; reactions were terminated with 0.5 M EDTA (pH 8.0). Detailed protocol is found in the Extended Experimental Procedures.

Chromatin Fractionation
Nuclei were extracted and digested with diluted MNase to yield DNA fragments with an average size larger than 20 Kbs. The fractionation was performed as described before (Gilbert et al., 2004) with more details presented in the Extended Experimental Procedures.

Fluorescence-Activated Cell Sorting of MOE Cell Populations
For FACS experiments, the olfactory epithelium of 6- to 10-week-old OMP-IRES-GFP, Ngn1-GFP, or P2-IRES-GFP mice was dissected and cells were dissociated using a papain dissociation kit (Worthington Biochemical, Freehold, NJ) following the manufacturer's instructions. See Extended Experimental Procedures for more details.

Transgene Mapping and X-Galactosidase Staining
Mapping of the OMP-LacZ transgene and staining of neurons with X-galactosidase were performed as per standard protocols. See Extended Experimental Procedures for more details.

SUPPLEMENTAL INFORMATION

Supplemental Information includes Extended Experimental Procedures, seven figures, and two tables and can be found with this article online at doi:10.1016/j.cell.2011.03.040.

Figure 6. The Active OR Allele Is Not Enriched for H3K9me3 or H4K20me3, but It Is Marked with H3K4me3

Heterozygote P2-IRES-GFP and MOR28-IRES-GFP mice were used to isolate GFP⁺ and GFP⁻ cells by FACS. ChIP experiments were performed in these cells with antibodies against H3K9me3 and H4K20me3 or against H3K4me3.

(A) The location of the primers used in this experiment is depicted here. Primers for the GFP sequence were used to specifically monitor the active allele, whereas the ORWT primers specifically amplified the inactive allele.

(B and C) GFP is hypomethylated on H3K9 (B) in the GFP⁺ cells, in which it is transcribed, but not in the GFP⁻ cells (C), in which this *P2* allele is inactive. The inactive allele, amplified specifically by the p2WT primers, shows high enrichment for H3K9me3 in both GFP⁺ and GFP⁻ populations. *Omp* and *Tbp* are used as negative controls and *Zfp560* and repeats (major satellite) as positive controls.

(D and E) As above, but the GFP⁺ cells from MOR28-IRES-GFP heterozygous mice were subject to a second round of FACS to yield a > 95% pure population and were then used for H3K9me3 ChIPs.

(F) Similar results were obtained for the H4K20me3 ChIPs with P2-GFP-sorted cells.

(G) We repeated the same ChIP-qPCR experiment with an antibody against H3K4me3. There is significant enrichment for H3K4me3 throughout the gene, but not on the neighboring *P3* gene or a distant OR (*Olfr177*) in the GFP⁺ cells. As expected, there was no H3K4me3 on the *P2* gene or any other OR gene in the GFP⁻ cells.

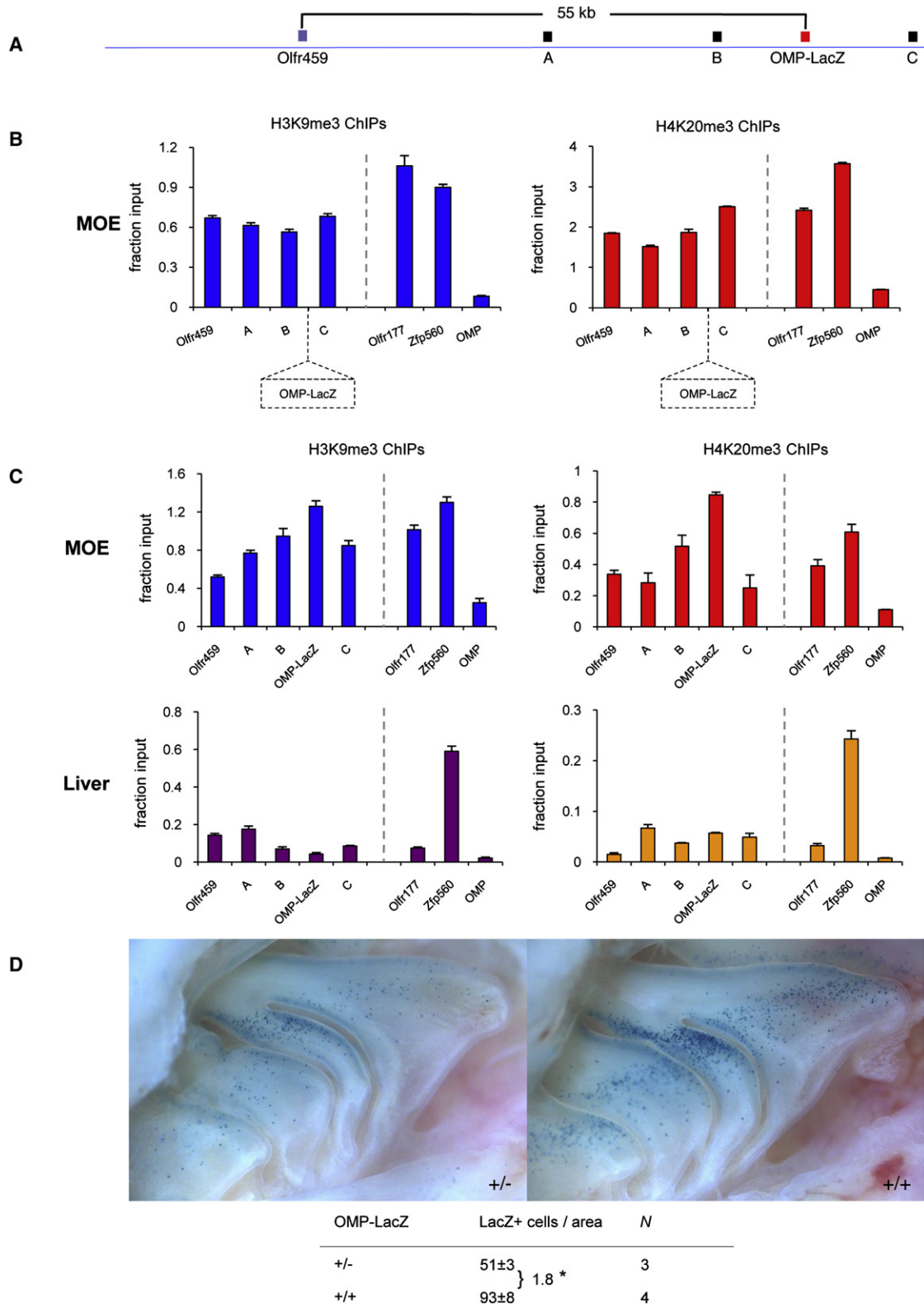Values are the mean of triplicate qPCR. Error bars represent the SEM. See also Figure S6.

Figure 7. Tissue-Specific OR Modifications Are Associated with OR-like Transgene Expression

(A) Graphic representation of the *Olfr459* locus and the OMP-LacZ insertion site located 55 kb away. Positions marked A, B, and C depict assayed regions in the qPCR analysis below.

REFERENCES

Axel, R. (2005). Scents and sensibility: a molecular logic of olfactory perception (Nobel lecture). Angew. Chem. Int. Ed. Eng. *44*, 6110–6127.

Barnea, G., O'Donnell, S., Mancia, F., Sun, X., Nemes, A., Mendelsohn, M., and Axel, R. (2004). Odorant receptors on axon termini in the brain. Science *304*, 1468.

Barski, A., Cuddapah, S., Cui, K., Roh, T.Y., Schones, D.E., Wang, Z., Wei, G., Chepelev, I., and Zhao, K. (2007). High-resolution profiling of histone methylations in the human genome. Cell *129*, 823–837.

Buck, L., and Axel, R. (1991). A novel multigene family may encode odorant receptors: a molecular basis for odor recognition. Cell *65*, 175–187.

Carter, L.A., MacDonald, J.L., and Roskams, A.J. (2004). Olfactory horizontal basal cells demonstrate a conserved multipotent progenitor phenotype. J. Neurosci. *24*, 5670–5683.

Cau, E., Casarosa, S., and Guillemot, F. (2002). Mash1 and Ngn1 control distinct steps of determination and differentiation in the olfactory sensory neuron lineage. Development *129*, 1871–1880.

Celniker, S.E., Dillon, L.A., Gerstein, M.B., Gunsalus, K.C., Henikoff, S., Karpen, G.H., Kellis, M., Lai, E.C., Lieb, J.D., MacAlpine, D.M., et al; modENCODE Consortium. (2009). Unlocking the secrets of the genome. Nature *459*, 927–930.

Chen, X., Fang, H., and Schwob, J.E. (2004). Multipotency of purified, transplanted globose basal cells in olfactory epithelium. J. Comp. Neurol. *469*, 457–474.

Chess, A., Simon, I., Cedar, H., and Axel, R. (1994). Allelic inactivation regulates olfactory receptor gene expression. Cell *78*, 823–834.

Dickson, J., Gowher, H., Strogantsev, R., Gaszner, M., Hair, A., Felsenfeld, G., and West, A.G. (2010). VEZF1 elements mediate protection from DNA methylation. PLoS Genet. *6*, e1000804.

Duggan, C.D., and Ngai, J. (2007). Scent of a stem cell. Nat. Neurosci. *10*, 673–674.

Dulac, C., and Axel, R. (1995). A novel family of genes encoding putative pheromone receptors in mammals. Cell *83*, 195–206.

Fodor, B.D., Shukeir, N., Reuter, G., and Jenuwein, T. (2010). Mammalian Su(var) genes in chromatin control. Annu. Rev. Cell Dev. Biol. *10*, 471–501.

Fuss, S.H., Omura, M., and Mombaerts, P. (2007). Local and cis effects of the H element on expression of odorant receptor genes in mouse. Cell *130*, 373–384.

Ghirlando, R., Litt, M.D., Prioleau, M.N., Recillas-Targa, F., and Felsenfeld, G. (2004). Physical properties of a genomic condensed chromatin fragment. J. Mol. Biol. *336*, 597–605.

Gilbert, N., Boyle, S., Fiegler, H., Woodfine, K., Carter, N.P., and Bickmore, W.A. (2004). Chromatin architecture of the human genome: gene-rich domains are enriched in open chromatin fibers. Cell *118*, 555–566.

Goldmit, M., and Bergman, Y. (2004). Monoallelic gene expression: a repertoire of recurrent themes. Immunol. Rev. *200*, 197–214.

Goldmit, M., Ji, Y., Skok, J., Roldan, E., Jung, S., Cedar, H., and Bergman, Y. (2005). Epigenetic ontogeny of the Igk locus during B cell development. Nat. Immunol. *6*, 198–203.

Guenther, M.G., Levine, S.S., Boyer, L.A., Jaenisch, R., and Young, R.A. (2007). A chromatin landmark and transcription initiation at most promoters in human cells. Cell *130*, 77–88.

Hawkins, R.D., Hon, G.C., Lee, L.K., Ngo, Q., Lister, R., Pelizzola, M., Edsall, L.E., Kuan, S., Luu, Y., Klugman, S., et al. (2010). Distinct epigenomic landscapes of pluripotent and lineage-committed human cells. Cell Stem Cell *6*, 479–491.

Heintz, N. (2004). Gene expression nervous system atlas (GENSAT). Nat. Neurosci. *7*, 483.

Imai, T., Sakano, H., and Vosshall, L.B. (2010). Topographic mapping—the olfactory system. Cold Spring Harb. Perspect. Biol. *2*, a001776.

Jang, W., Kim, K.P., and Schwob, J.E. (2007). Nonintegrin laminin receptor precursor protein is expressed on olfactory stem and progenitor cells. J. Comp. Neurol. *502*, 367–381.

Kim, T.H., Abdullaev, Z.K., Smith, A.D., Ching, K.A., Loukinov, D.I., Green, R.D., Zhang, M.Q., Lobanenkov, V.V., and Ren, B. (2007). Analysis of the vertebrate insulator protein CTCF-binding sites in the human genome. Cell *128*, 1231–1245.

Larson, J.L., and Yuan, G.C. (2010). Epigenetic domains found in mouse embryonic stem cells via a hidden Markov model. BMC Bioinformatics *11*, 557.

Leung, C.T., Coulombe, P.A., and Reed, R.R. (2007). Contribution of olfactory neural stem cells to tissue maintenance and regeneration. Nat. Neurosci. *10*, 720–726.

Lewcock, J.W., and Reed, R.R. (2004). A feedback mechanism regulates monoallelic odorant receptor expression. Proc. Natl. Acad. Sci. USA *101*, 1069–1074.

Liberles, S.D., Horowitz, L.F., Kuang, D., Contos, J.J., Wilson, K.L., Siltberg-Liberles, J., Liberles, D.A., and Buck, L.B. (2009). Formyl peptide receptors are candidate chemosensory receptors in the vomeronasal organ. Proc. Natl. Acad. Sci. USA *106*, 9842–9847.

Lomvardas, S., Barnea, G., Pisapia, D.J., Mendelsohn, M., Kirkland, J., and Axel, R. (2006). Interchromosomal interactions and olfactory receptor choice. Cell *126*, 403–413.

McIntyre, J.C., Bose, S.C., Stromberg, A.J., and McClintock, T.S. (2008). Emx2 stimulates odorant receptor gene expression. Chem. Senses *33*, 825–837.

Nguyen, M.Q., Zhou, Z., Marks, C.A., Ryba, N.J., and Belluscio, L. (2007). Prominent roles for odorant receptor coding sequences in allelic exclusion. Cell *131*, 1009–1017.

Nishizumi, H., Kumasaka, K., Inoue, N., Nakashima, A., and Sakano, H. (2007). Deletion of the core-H region in mice abolishes the expression of three proximal odorant receptor genes in cis. Proc. Natl. Acad. Sci. USA *104*, 20067–20072.

O'Geen, H., Squazzo, S.L., Iyengar, S., Blahnik, K., Rinn, J.L., Chang, H.Y., Green, R., and Farnham, P.J. (2007). Genome-wide analysis of KAP1 binding suggests autoregulation of KRAB-ZNFs. PLoS Genet. *3*, e89.

Pellegrini, M., Mansouri, A., Simeone, A., Boncinelli, E., and Gruss, P. (1996). Dentate gyrus formation requires Emx2. Development *122*, 3893–3898.

Pyrski, M., Xu, Z., Walters, E., Gilbert, D.J., Jenkins, N.A., Copeland, N.G., and Margolis, F.L. (2001). The OMP-lacZ transgene mimics the unusual expression

(B) ChIP-qPCRs with chromatin from the MOE of wild-type mouse show that the *Olfr459* is enriched for H3K9me3 and H4K20me3, and both modifications appear to extend to the insertion site.
(C) ChIP-qPCR analysis of the MOE and liver from OMP-LacZ-positive animals. Both H3K9me3 and H4K20me3 show MOE-specific deposition on *Olfr459*, the OMP-LacZ transgene, and the regions proximal to these loci. Experiment was performed in two biological replicates with similar results. Values shown here are the mean of triplicate qPCRs. Error bars represent the SEM.
(D) X-gal stains of lateral whole mounts of the nasal cavities from hemizygote and homozygote OMP-LacZ animals. *N*, number of biological replicates. *$p < 10^{-4}$, Student's t test.
See also Figure S7.

pattern of OR-Z6, a new odorant receptor gene on mouse chromosome 6: implication for locus-dependent gene expression. J. Neurosci. *21*, 4637–4648.

Regha, K., Sloane, M.A., Huang, R., Pauler, F.M., Warczok, K.E., Melikant, B., Radolf, M., Martens, J.H., Schotta, G., Jenuwein, T., and Barlow, D.P. (2007). Active and repressive chromatin are interspersed without spreading in an imprinted gene cluster in the mammalian genome. Mol. Cell *27*, 353–366.

Rivière, S., Challet, L., Fluegge, D., Spehr, M., and Rodriguez, I. (2009). Formyl peptide receptor-like proteins are a novel family of vomeronasal chemosensors. Nature *459*, 574–577.

Rothman, A., Feinstein, P., Hirota, J., and Mombaerts, P. (2005). The promoter of the mouse odorant receptor gene M71. Mol. Cell. Neurosci. *28*, 535–546.

Royce-Tolland, M., and Panning, B. (2008). X-inactivation: it takes two to count. Curr. Biol. *18*, R255–R256.

Sammeta, N., Yu, T.T., Bose, S.C., and McClintock, T.S. (2007). Mouse olfactory sensory neurons express 10,000 genes. J. Comp. Neurol. *502*, 1138–1156.

Scherf, A., Lopez-Rubio, J.J., and Riviere, L. (2008). Antigenic variation in Plasmodium falciparum. Annu. Rev. Microbiol. *62*, 445–470.

Serizawa, S., Miyamichi, K., Nakatani, H., Suzuki, M., Saito, M., Yoshihara, Y., and Sakano, H. (2003). Negative feedback regulation ensures the one receptor-one olfactory neuron rule in mouse. Science *302*, 2088–2094.

Shykind, B.M. (2005). Regulation of odorant receptors: one allele at a time. Hum. Mol. Genet. *14*(Spec No 1), R33–R39.

Shykind, B.M., Rohani, S.C., O'Donnell, S., Nemes, A., Mendelsohn, M., Sun, Y., Axel, R., and Barnea, G. (2004). Gene switching and the stability of odorant receptor gene choice. Cell *117*, 801–815.

Song, J.S., Johnson, W.E., Zhu, X., Zhang, X., Li, W., Manrai, A.K., Liu, J.S., Chen, R., and Liu, X.S. (2007). Model-based analysis of two-color arrays (MA2C). Genome Biol. *8*, R178.

Trojer, P., and Reinberg, D. (2007). Facultative heterochromatin: is there a distinctive molecular signature? Mol. Cell *28*, 1–13.

Walters, E., Grillo, M., Oestreicher, A.B., and Margolis, F.L. (1996). LacZ and OMP are co-expressed during ontogeny and regeneration in olfactory receptor neurons of OMP promoter-lacZ transgenic mice. Int. J. Dev. Neurosci. *14*, 813–822.

Weintraub, H., and Groudine, M. (1976). Chromosomal subunits in active genes have an altered conformation. Science *193*, 848–856.

Wen, B., Wu, H., Shinkai, Y., Irizarry, R.A., and Feinberg, A.P. (2009). Large histone H3 lysine 9 dimethylated chromatin blocks distinguish differentiated from embryonic stem cells. Nat. Genet. *41*, 246–250.